Polymer 54 (2013) 6177–6183

Contents lists available at ScienceDirect

Polymer

journal homepage: www.elsevier.com/locate/polymer

Superhard transparent hybrid nanocomposites for high fidelity UV-nanoimprint lithography

Marina A. González Lazo, Maïté Blank, Yves Leterrier*, Jan-Anders E. Månson

Laboratoire de Technologie des Composites et Polymères (LTC), Ecole Polytechnique Fédérale de Lausanne (EPFL), CH-1015 Lausanne, Switzerland

ARTICLE INFO

Article history:
Received 24 June 2013
Received in revised form
4 September 2013
Accepted 5 September 2013
Available online 12 September 2013

Keywords:
Hyperbranched polymer
Hybrid nanocomposites
UV nanoimprint lithography

ABSTRACT

Transparent hyperbranched acrylate nanocomposites were produced using different combinations of silica nanoparticles and silicon-based sol–gel precursors. The nanocomposites were processed using a dual-cure UV polymerization and condensation scheme. The viscosity of hybrid suspensions was found to be one to two orders of magnitude lower than that of particulate composites with the same equivalent silica fraction. The Vickers microhardness of the polymer was 112 MPa. It was equal to 190 MPa and 148 MPa for the hybrid composites and particulate composites with 20 vol% SiO_2, respectively, and it was equal to 287 MPa for the hybrid material with 30 vol% SiO_2. Light-trapping textures in the form of random sub-micron pyramidal features were replicated in the hybrid composites from a nickel template using UV-nanoimprint lithography. After optimization of the dual-cure process sequence, a very high replication fidelity was obtained for all investigated compositions, leading to a haze above 99% over the visible light spectrum and a very effective light scattering performance in a broad angular exposure.

1. Introduction

Hybrid materials based on a combination of organic and inorganic precursors and produced using sol–gel processes have emerged in the last two decades and stimulated numerous research efforts as recently reviewed by Drisko and Sanchez [1]. Polymer nanocomposites based on preformed nanoparticles mixed with the polymer also enjoy great attention, with a focus on enhanced thermo-mechanical performance [2]. For both sol–gel and particulate composite materials the combination of organic and inorganic phases and their interactions give rise to outstanding mechanical properties such as toughness [3] and microhardness [4], diffusion barrier properties, flexibility and optical transparency [5,6]. Precursors are also often low cost and are compatible with cost-effective processing methods, including photopolymerization and roll-to-roll (R2R) processing [7,8]. These attributes make such nanocomposite materials good candidates for the encapsulation of flexible devices as OLEDs [5] or thin film silicon solar cells [9].

The numerous benefits of particulate nanocomposites depend on a good dispersion of the nanoparticles. Avoiding particle agglomeration is challenging and often requires tailored particle surface modification. Another problem is related to the very large specific interfacial area. In this case, even small amounts of nanoparticles may drastically increase the viscosity of the composite, so the liquid-like polymer is transformed into a solid-like composite. As an example, it was found that the addition of 5 vol % of 12 nm diameter silica nanoparticles to an acrylate monomer led to gelation of the suspension, and that at 20 vol% of nanoparticles the viscosity increased by more than five orders of magnitude [10]. Such processing problems can be overcome by using solvents. An alternative is, in fact, the sol–gel route, whereby the liquid inorganic precursors enable a low viscosity of the hybrid solution to be maintained, thus avoiding the problematic liquid-to-solid transition of the particulate suspensions. This process moreover enables a very homogeneous dispersion of the reactants at the molecular level, hence of the inorganic phase within the polymerized matrix [8,11–14]. The resulting sol–gel composites are thus very versatile since the contributions of the organic and inorganic phases and their interactions can be carefully tailored. This enables accurate control of a broad range of properties, particularly for optical and protective coating applications [11,15]. However, the mechanical properties of the sol–gel composites are lower than those obtained with particulate composites, since the inorganic component acting as a network former does not contribute to the material properties based on its physical state properties [8,16] to the same degree as in the case of preformed nanoparticles.

Focus of the present work is on the development of light-trapping textures based on hybrid silica-hyperbranched polymer

* Corresponding author.
E-mail address: yves.leterrier@epfl.ch (Y. Leterrier).

0032-3861/$ – see front matter © 2013 Elsevier Ltd. All rights reserved.
http://dx.doi.org/10.1016/j.polymer.2013.09.004

(HBP) nanocomposites. HBPs are globular molecules with high reactivity and Newtonian viscosity [17], low polymerization shrinkage [18] and good compatibility with inorganic components [19,20]. Particulate and sol–gel nanocomposites based on a UV-curable HBP with improved thermomechanical stability and hardness compared to the unreinforced HBP have been reported in recent works [9,18]. Moreover, these nanocomposite materials enabled sub-micron sized structures to be replicated with a very high fidelity using UV nanoimprint lithography (UVNIL) owing to their low shrinkage. The low pressure, low temperature and short time needed to create nanocomposite replicas using UVNIL are all favorable for implementation in printing industries [21]. However, the liquid-to-solid transition of particulate nanocomposites at low particle fraction, or the long condensation time of sol–gel nanocomposites might invalidate the UVNIL process. The objective of the present work was thus to explore an alternative route, with the aim of achieving a balanced viscosity between the particulate and sol–gel cases, while minimizing the process cycle time and maximizing the mechanical properties of the final material. The approach was to combine nanoparticles, HBP and sol–gel precursors to form multi-scale hybrid nanocomposites (e.g. Refs. [8,16]). The combination of controlled rheology and high hardness should be advantageous for the fast production of hard coats, and of functional coatings with tailored surface textures.

2. Experimental section

2.1. Materials and processing

The HBP was a polyester acrylate oligomer with a functionality of 16, a density of 1.13 g/cm^3 and a glass transition temperature in cured state equal to 165 °C (CN2302, Sartomer). The photo-initiator was 2,4,6Trimethylbenzoyldiphenyl phosphine oxide (Esacure TPO, Lamberti). The nanoparticles were methacrylated amorphous fumed SiO_2 in the form of nanopowder aggregates with a primary particle size of 12 nm and a specific surface area of about 150 m^2/g (Aerosil R7200, Evonik). The organometal precursor was tetraethylorthosilicate (TEOS, Sigma–Aldrich). Methacryloxy(propyl)trimethoxysilane (MEMO, Sigma–Aldrich) was used as a coupling agent.

Three different nanocomposites were developed, namely particulate composites, sol–gel composites and hybrid composites; their composition is detailed in Table 1. In all cases the photo-initiator was first dissolved in the HBP at 75 °C at a concentration of 6 wt% and stirred for 15 min. Following references to HBP will always refer to the mixture of HBP with 6 wt% photoinitiator.

Particulate composites were prepared by solvent-assisted mixing of the HBP with the methacrylated silica particles. The particles were first dispersed in isopropanol (ratio 1:3 by weight) and sonicated to disagglomerate the aggregates (400 W, Digital Sonifier, Branson). A selected amount of SiO_2 suspension was then added to the HBP and the mixture was stirred for 1 h. The corresponding particle volume fraction was calculated assuming a density of 2.2 g/cm^3 for fused silica. The solvent was then evaporated at 60 °C under vacuum until no more weight variation of the suspension was detected. Particulate composites with up to 30 vol% of SiO_2 were prepared.

Sol–gel composites were produced in three steps, by mixing the HBP with MEMO first, then adding TEOS, and finally 1 M HCl in water (Sigma–Aldrich). Acidic conditions (pH $\leq$ 2 in the present case) combined with the presence of the coupling agent ensured the formation of a fine silica network rather than aggregates [18]. After each step the mixture was stirred at room temperature until homogenization was visually observed. After addition of HCl the mixture was further stirred for 30 min. Composites with up to 20 vol% of silica were prepared. The volume fraction of SiO_2 in the cured composite was calculated assuming a density of 2.0 g/cm^3 for the sol–gel silica. A corresponding amount of TEOS was calculated assuming 100% conversion of the precursor into SiO_2. The amount of coupling agent was calculated to give a concentration of 10% methacrylic groups within acrylic groups. Conversion of the silanol groups into SiO_2 was also assumed to be 100%. The amount of H_2O was calculated to give a molar ratio of H_2O to ethyl groups equal to 1:2.

Hybrid composites were prepared by combining the direct mixing and sol–gel processes, using both silica particles and a liquid silica precursor. A suspension of the methacrylated silica nanoparticles in the HBP was prepared first as described above for the particulate composites. MEMO and TEOS were subsequently mixed with the suspension and the mixture was stirred until homogenization was visually observed. 1 M HCl in H_2O was eventually added and the hybrid suspension was further stirred for 30 min. Composites with up to 30 vol% of silica, including up to 20 vol% of silica resulting from the condensation of TEOS were prepared. The volume fraction of silica in the suspensions and in the cured composites was the sum of the particles fraction and the sol–gel silica fraction. In the case of the suspensions, the volume fraction of silica should be considered as an equivalent fraction to enable comparison with the particulate suspensions.

It was found that the hybrid suspensions containing an increasing concentration of TEOS were less stable and gelled faster when stored at ambient temperature for several days. It was in fact shown that for solutions having a pH lower than the isoelectric pH, namely 2.2 for silica, the gel time decreased with the acidity of the solution [12]. This explains the differences of stability that we observed, since the acidity of the solution increased with the amount of TEOS (the HCl:TEOS ratio was kept constant). Sol-gel

Table 1
Composition of particulate, sol–gel and hybrid composites and dual-cure process timing for sol–gel and hybrid composites. Dashes indicate that no coatings were produced.

Composite abbreviation	SiO_2 nanoparticles [wt%]	SiO_2 nanoparticles [vol%]	TEOS [wt%]	MEMO [wt%]	Silica from TEOS [vol%]	Condensation time before UV-polymerization [min]	Total condensation time [h]
5A	9.3	5	0	0	0	–	–
5T	0	0	13.8	8.5	5	240	4
10A	17.8	10	0	0	0	–	–
10T	0	0	24.8	6.9	10	240	4
5A_5T	9.6	5	12.5	7.7	5	–	–
3A_10T	6	3	23.3	6.5	10	2, 6, 15, 30, 45	4
5A_10T	9.8	5	22.3	6.3	10	–	–
20A	32.7	20	0	0	0	–	–
20T	0	0	39.6	4.8	20	240	4
10A_10T	18.7	10	20.2	5.6	10	30, 45	4
5A_20T	10.1	5	35.2	4.4	20	6, 8[a], 10[a]	1, 4
30A	45.5	30	0	0	0	–	–
10A_20T	19.3	10	31.6	3.9	20	6	4

[a] Replication fidelity not very high.

reactions are thermally activated and storing the solutions in a cold atmosphere rather than at ambient temperature can strongly enhance their stability [12,22,23]. In the present study, the rheological tests were performed within few hours after preparation i.e., well before gelation.

A 200 W mercury bulb UV lamp (OmniCure 2000, Exfo, Canada) was used to cure all composites. The light intensity was measured using a calibrated radiometer (Silver Line, CON-TROL-CURE, Germany), between 230 and 410 nm. All samples were irradiated during 3 min using a UV intensity of 130 mW/cm^2 for flat samples and of 75 mW/cm^2 for textured samples. For sol–gel and hybrid composites, a dual-cure (sol–gel condensation and photopolymerization) process was used [11,15]. Condensation of the inorganic phase was achieved at 80 °C during 1 or 4 h. Photopolymerization occured either during or after the whole condensation process, as indicated in Table 1.

Light trapping textures were fabricated in the hybrid composites using a UVNIL tool as detailed in a previous work [9]. A Ni master in the form of a 24 mm × 24 mm square foil was used, with random sub-micron pyramidal structures replicated from ZnO crystals was used. Using this random structure, texturization of the back reflector in a thin film silicon solar cell enabled the photocurrent to be increased by 23% [9,24]. The hybrid solutions were deposited either on a glass slide or on a 50 μm thick polyethylene naphthalate (PEN) substrate, and subsequently polymerized using the dual-cure process sequences summarized in Table 1. Samples were placed in an oven at 80 °C for the condensation process. After a certain time, the Ni master was placed on the partially condensed sample and the assembly was loaded into the UVNIL tool. A pressure of 3 bars was applied while UV polymerization was performed. The texturized sample was finally put back in the oven at 80 °C to complete the condensation process.

In the following, the suspensions and cured composites will be referred to as *x*A, *x*A_*y*T and *x*A_*y*T_$z_1$min_z_2h, where *x* and *y* are the volume fraction of Aerosil nanoparticles 'A' and silica obtained from the condensation of TEOS 'T', respectively; z_1 is the onset time in min for UV polymerization with respect to the start of the condensation reaction at 80 °C and z_2 is the total condensation time in hours.

2.2. Characterization methods

Rheological measurements of the various mixtures were conducted in a rheometer (AR2000, TA instruments) with plate–plate geometry. The plate diameter was either 25 mm or 40 mm, depending on the sample viscosity. The distance between the plates was set to 100 μm. For each sample, the linear viscoelastic range was determined through strain sweep tests at a frequency of 1 Hz. Frequency sweep tests were then performed. Evaporation of sol–gel precursors was avoided using a solvent trap cover.

The microhardness of each composite was measured using a Vickers indenter (Miniload microhardness tester, Leitz, Germany). Coatings with thicknesses of 150–200 μm on glass slides were indented using a weight of 50 g during 15 s. A weight of 500 g was used for the 10A_20T hybrid composite due to its high hardness. At least five indentations were made on each sample and the hardness was determined from optical micrographs with an Olympus BX60 optical microscope. Differential interference contrast illumination was used to maximize contrast in the transparent composites. The two diagonals (typically 100 μm) of the pyramidal indentation were measured with ~1 μm accuracy. The hardness *H* (in MPa) was calculated as:

$$H = 1.854\,P/d^2 \quad (1)$$

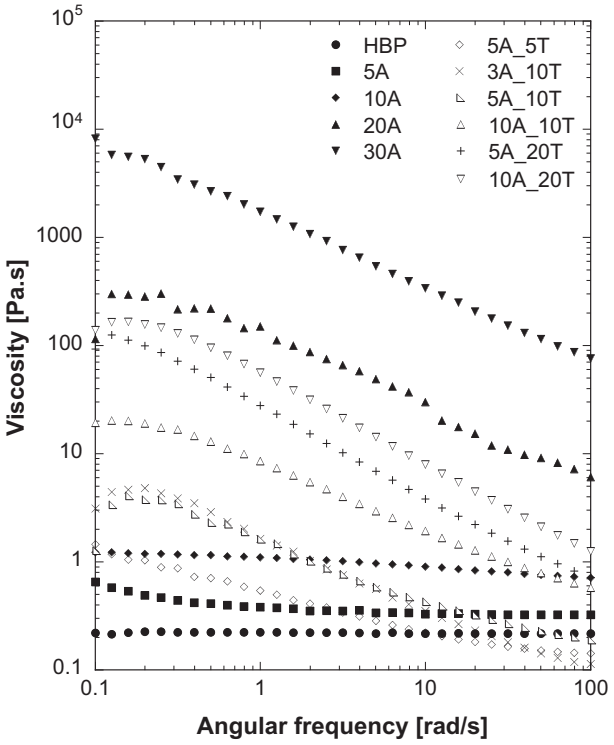

Fig. 1. Viscosity of composites as function of angular frequency. Composites are denominated based on their composition *x*A and *x*A_*y*T, where *x* and *y* are the volume fractions of Aerosil nanoparticles 'A' and silica obtained from the condensation of TEOS 'T', respectively.

where *P* is the force (in *N*) and *d* is the mean diagonal length of the indentation (in mm). The factor 1.854 comes from the geometry of the pyramidal indenter with a face angle equal to 136°.

The topography of the texturized samples was examined by scanning electron microscopy (SEM, FEI XL30-SFEG) in ultra-high resolution mode using an acceleration voltage of 10 kV. The working distance was usually 10 mm. In order to avoid any charging effect, the samples were covered with a 25 nm thick carbon layer.

The haze parameter (ratio of scattered light to total reflected light) was measured with a Perkin Elmer UV/VIS/NIR Spectrometer Lambda 900 in reflection mode. Angle-resolved scattering (ARS) of light was measured with a detector on a goniometer under normal incidence onto the sample surface, using a laser at a wavelength of 543 nm [25]. In both cases, a 200 nm thick silver layer was sputtered onto the texturized samples prior to optical characterization.

3. Results and discussion

3.1. Rheological behavior

The viscosity of the HBP and of particulate and hybrid suspensions is depicted in Fig. 1. The HBP showed Newtonian behavior, with a viscosity independent of frequency and equal to 0.2 Pa.s. The viscosity of suspensions of acrylated SiO_2 nanoparticles in HBP rapidly increased with increasing nanoparticle loading and shear thinning became evident at particle concentrations of 5 vol% and above. This thixotropic behavior resulted from the break-down of particulate aggregates and release of the immobilized liquid with increasing shear rate [22]. At 30 vol% of silica the viscosity of the particulate suspension at low frequency was close to 10 000 Pa.s, almost 5 orders of magnitude higher than that of the HBP. Such a dramatic increase in viscosity is associated with a liquid-to-solid

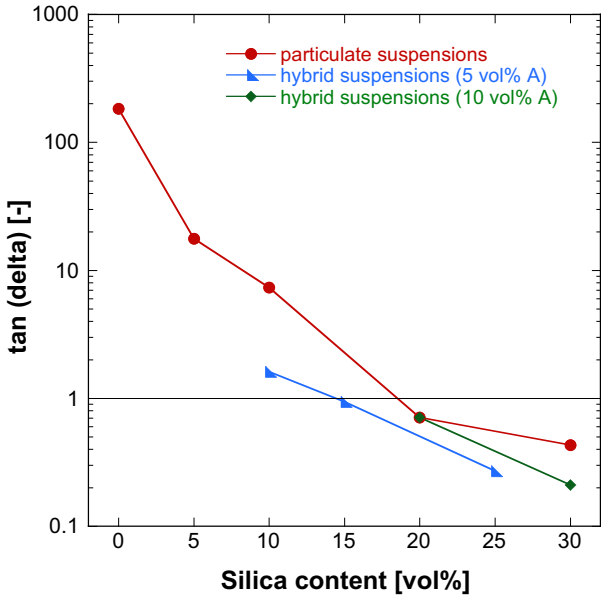

Fig. 2. Tangent of the phase angle of nanocomposites vs. silica content at an angular frequency of 6.3 rad/s. The black line represents the liquid-to-solid transition.

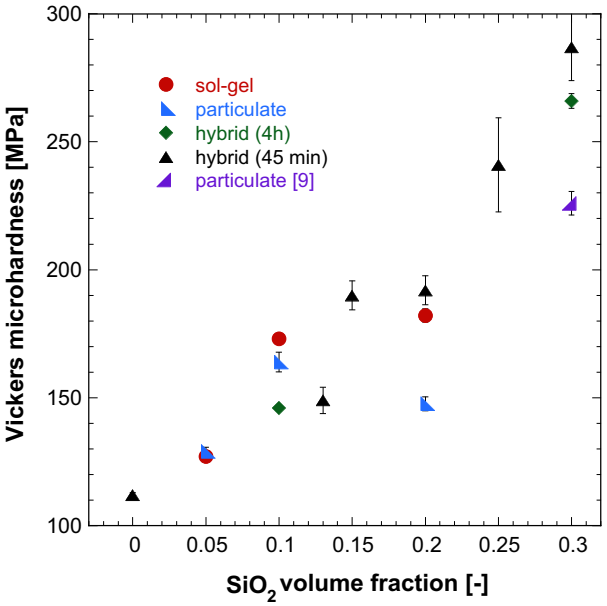

Fig. 3. Vickers microhardness of HBP-SiO_2 particulate, sol–gel and hybrid composites vs. SiO_2 volume fraction. For hybrid composites, results are shown for polymerization after 45 min or after 4 h, for a total condensation time of 4 h. The hardness of a particulate composite based on monodisperse SiO_2 from Ref. [9] is shown for comparison.

transition, and results from the formation of a gel-type network [10].

The viscosity of the hybrid suspensions also increased with increasing fraction of nanoparticles. They exhibited a thixotropic behavior similar to their particulate counterparts [26], rather than that of their sol–gel counterparts, which is Newtonian [7]. Nevertheless the presence of the sol–gel precursor considerably changed the behavior of the suspensions, with the occurrence of shear thinning at low particle fraction, and with a large decrease of viscosity for a given silica fraction, compared to that of the particulate suspensions. For example, the particulate suspension 10A was quasi Newtonian with moderate thinning whereas the hybrid suspension 5A_5T (i.e., with same final volume fraction of silica) was clearly thinning. The suspension 30A and hybrid suspension 10A_20T (again, with the same final fraction of silica) were both shear thinning with a comparable exponent, but the viscosity of the latter was 40 times lower. Interestingly, increasing the amount of TEOS for a given fraction of nanoparticles led to an unexpected increase of viscosity: solutions 5A_5T, 5A_10T and 5A_20T had viscosities (at 0.1 rad/s) of 1.5, 3.4 and 92.5 Pa.s, and solutions 10A_10T and 10A_20T have viscosities of 20 Pa.s and 200 Pa.s, respectively. This result was surprising since the viscosity of TEOS/HBP solutions was found to decrease in proportion with the amount of TEOS owing to its lower viscosity compared to that of the organic monomer [7].

This unexpected increase of viscosity in fact reflects the considerable influence of interfacial interactions in the hybrid suspensions and related dispersion state of the nanoparticles [27]. Interfacial interactions dominate the viscous response of systems with very high interfacial areas (i.e., nanoparticles with specific surfaces above 100 m^2/g at volume fractions above few %) [10]. Upon hydrolysis of the TEOS, the $Si(OH)_4$ molecules will tend to attach via H-bonding to the methacrylate ends of the silane molecules at the surface of the silica particles. Assuming that the number density of silanol groups on amorphous silica is equal to 6 nm^{-2} [28] and that the silylation of the silica particles (with a specific surface of 150 m^2/g) was quantitative, the minimum concentration of $Si(OH)_4$ in the solution to fully H-bond one of the (OH) with the methacrylated surface of all particles at a particle concentration of 1 vol% would be equal to 0.14 vol%. In the present work the concentration of TEOS in the solution was always greater than or equal to that of silica particles, so it can be assumed that the entire surface of each particle was covered by a shell of $Si(OH)_4$ molecules. The volume of the 6 nm radius particles decorated with a shell of $Si(OH)_4$ with molecular diameter of approximately 2 nm is almost 2.5 times larger than the volume of the particles without the $Si(OH)_4$ shell. Therefore, the effective volume fraction [10] of silica particles in the hybrid suspensions also increased by almost 2.5 times due to the adsorption of $Si(OH)_4$. This considerable increase of effective particle concentration dramatically impacted the rheological behavior. This effect is illustrated in Fig. 2 where the tangent of the phase angle (i.e., the ratio of the loss modulus to the storage modulus) of the different suspensions is shown as a function of the silica content at an angular frequency of 6.3 rad/s. It should be stressed that for the hybrid suspensions the silica content refers to the final volume fraction of silica in the cured composites. The liquid-to-solid transition takes place when tan (δ) is equal to one (gelation). The phase angle of the HBP was equal to 200, far into the liquid like domain. With increasing silica concentration, the phase angle of the particulate suspensions rapidly decreased, reaching a value of 20 at 5 vol% of silica, and crossing the gelation limit at a concentration around 18 vol%. At 20 vol% and above the particulate suspensions were in a gel state. The phase angle of the hybrid suspension with a fixed amount of silica particles of 5 vol% decreased also rapidly with increasing concentration of TEOS, being always lower than that of the particulate analog, crossing the gelation line at a concentration of 15 vol% of silica. The premature gelation of the hybrid suspension was the consequence of the immobilization of the silica particle network due to H-bonding between the methycrylate surface of the particles and the $Si(OH)_4$ molecules.

3.2. Microhardness

Fig. 3 shows the microhardness of particulate, sol–gel and hybrid composites as a function of silica fraction and process timing for the hybrid composites.

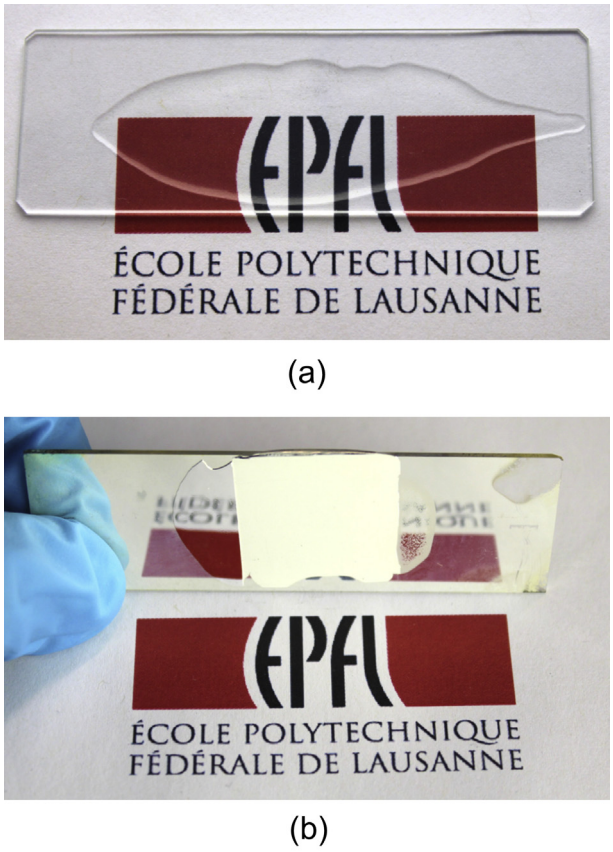

Fig. 4. Pictures of a 200 μm thick 10A_20T hybrid composite coating on a glass slide placed on a printed paper support (a) and of a textured 10A_10T hybrid composite coating on a glass slide with a 200 nm top silver coating (b). Mirror effect (specular reflection) is evident on the flat surfaces, while light scattering (diffuse reflection) is evident in the textured square in the center.

The hardness of HBP was equal to 112 MPa. It increased to a value of 164 MPa for the particulate composite containing 10 vol% of silica, but then decreased to 148 MPa at 20 vol% of silica, presumably due to the presence of porosities. In fact, with increasing particle loading, aggregates tend to form in the composite, and air entrapment often occurs due to the huge increase in viscosity, leading to an overall decrease in mechanical performance [3]. These issues were overcome in a recent work using a high compaction pressure, leading to a hardness value of 226 MPa at 30 vol% of silica (data shown in Fig. 3). This high value was also obtained due to the better dispersion state of the particles [9]. The hardness of the sol–gel composites also increased with silica fraction, reaching a value of 179 MPa for 20 vol% silica. In this case the in-situ formation of the silica phase prevented the incidence of the agglomeration problem and the low viscosity of the precursor mixture avoided air entrapment. It was moreover evident that the hardness increase between 10 vol% and 20 vol% of silica was much less than between 0 and 10 vol% of silica. This reduction in increase rate was attributed to the tensile stress resulting from condensation shrinkage, which was expected to increase with inorganic fraction. A higher tensile stress in the sol–gel coatings, particularly in the superficial layers, would lead to a lower hardness. In addition, one may invoke the occurrence of phase separation between organic and inorganic components when higher amounts of inorganic precursor are introduced in the system. The resulting formation of heterogeneous microstructures with weaker interfaces would also contribute to a reduction of the hardness [6]. Above 20 vol% the viscosity of the sol–gel solution was too low to make a coating thick enough for the test.

In the case of hybrid composites, hardness values also increased with the amount of both types of silica in the composite. The hardness of hybrid composites containing 13 to 20 vol% of SiO_2 was found to be similar to that of the two other composites. At the maximum investigated silica fraction of 30 vol% the hybrid composite with 10 vol% of particles +20 vol% of silica from TEOS was harder (287 MPa) than the particulate composite with 30 vol% of monodisperse silica particles (226 MPa) [9], while maintaining a considerably lower suspension viscosity. The hybrid composite polymerized after 45 min of condensation was also slightly harder than that polymerized after 4 h of condensation. This result is consistent with the lower internal tensile stress in the 45 min composite [18].

3.3. Light scattering textures

Fig. 4 shows UV cured hybrid composite coatings without and with an imprinted texture. All composites were transparent and homogeneous as shown for instance in the case of a total silica content of 30 vol% (10 vol% of particles + 20 vol% of silica from TEOS). Fig. 4 also demonstrates the light scattering effect of the textured surface, which was rendered obvious after sputtering a thin silver layer. The silver layer created a mirror effect on the flat surfaces of the sample. However it took on the appearance of a white surface due to the diffuse reflection of incident light on the ZnO like random nanostructures.

The key to achieving a very high replication fidelity in the hybrid composites using a pressure as low as 3 bars was the timing of the dual-cure process, as was concluded in a recent work [18]. When UVNIL was performed first, the subsequent condensation shrinkage generated a high stress resulting in cracking of the composite. When condensation was performed first, followed by UVNIL, evaporation shrinkage occurred in the liquid material and no shrinkage stress built up. However, the high viscosity of the silica-forming network compromised the processability of the composite and its resulting replication fidelity. An optimal sequence for the two processes, in which UVNIL was carried out some time after the condensation reaction had started, was thus devised for each composition in order to benefit from the low viscosity for processing without cracking of the polymerized material. For a given amount of TEOS, series of samples with increasing onset times for UVNIL with respect to the start of the condensation were prepared. The optimal timing was defined as the shortest onset time where haze effect was observed. A higher content of TEOS led to a faster gelation [12], which resulted in a material that became hard quicker. The condensation time prior to UVNIL was therefore reduced for compositions with increasing amount of TEOS, so that imprinting could be done before gelation. It turned out that the optimal timing for a given composition was systematically the shortest of all investigated onset times, but it was always several minutes or more. Reducing the onset time to zero (UVNIL first) led to cracking problems during subsequent condensation.

Fig. 5 shows the morphology of the Ni master, the HBP and several composite replicas obtained with the optimal timing of the dual cure process. It is evident that in all cases the texture was replicated with no visible difference between the different materials. The fidelity of the replication process was quantified from the optical characterization of the textures.

Figs. 6 and 7 compare the haze and reflectance, and the ARS behavior, respectively, of the nickel master, HBP and hybrid composite replica, again produced with the optimal dual-cure process sequence. It is evident that all replicas mimic almost perfectly the haze behavior of the master for all wavelengths, with a haze above 99% in the investigated 400–800 nm range. The total reflectance measurement revealed no significant drop in the quantity of light collected by the photodetector. A similar tendency was found for

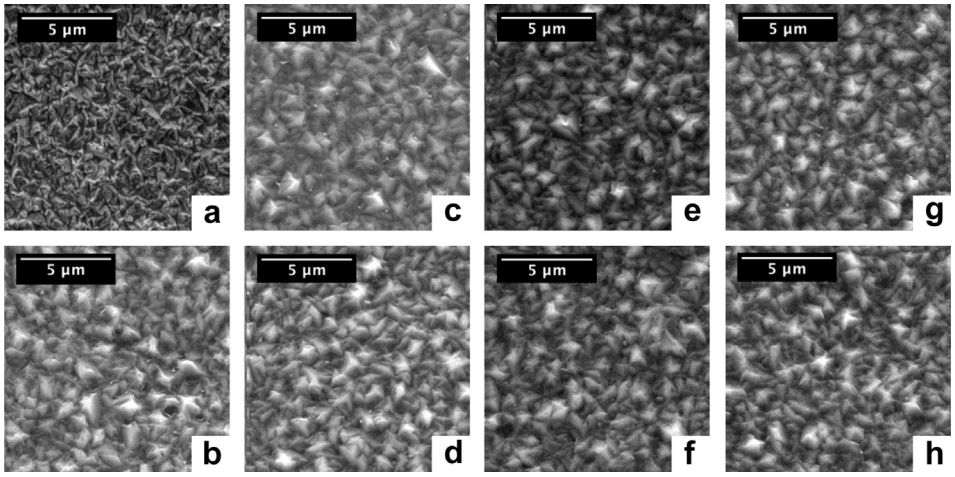

Fig. 5. SEM pictures of the nickel master (a), HBP replicate (b) and composite replicates 3A_10T with polymerization after 2 min (c), 10A_10T with polymerization after 30 min (d), 3A_10T with polymerization after 6 min (e), 10A_10T with polymerization after 45 min (f), 3A_10T with polymerization after 15 min (g) and 5A_20T with polymerization after 6 min (h). In all composite cases the total condensation time was 4 h.

ARS measurements depicted in Fig. 7 (the absence of a signal for scattering angles between −10° and +10° corresponds to the specular reflection). The scattering was identical to that of the master, and was very high in a broad angular exposure. The ARS signal was more than 50% of the maximum signal for scattering angles between −50° and +50° and more than 25% between −70° and +70°, which is comparable [29] or better [30] to the performance found for other ZnO replicas. These results are in contrast to the case of particulate composite replica, for which process-induced shrinkage stress led to a slight distortion of the texture and a reduction of the reflectance and ARS performance [9]. In the present case the limited drop in reflectance and maintained ARS performance are consistent with the reduction of the shrinkage stress observed in similar hybrid composites compared to that of particulate composites [18]. An attempt was made to reduce the total condensation time from 4 h to 1 h for the formulation 5A_20T. The optical performance for a total condensation time of 1 h was found to be identical to that for 4 h. Further reduction of the condensation time for such diffusion controlled process was not investigated but should be possible for thin coatings.

To summarize, the hybrid suspensions with considerably lower viscosity compared to their particulate analogs enable low-pressure processing and the patterning of composite coatings with a high silica fraction and resulting very high hardness. Such hybrid nanocomposites represent cost-effective materials for a broad range of applications including anti-scratch transparent coatings, large area light trapping textures for solar cells using R2R replication, and a number of optoelectronic devices such as waveguides on flexible substrates [31].

4. Conclusions

Hybrid HBP/silica nanocomposites were prepared using a combination of silica nanoparticles and sol–gel precursors, in a dual-cure photopolymerization and condensation process. The viscosity

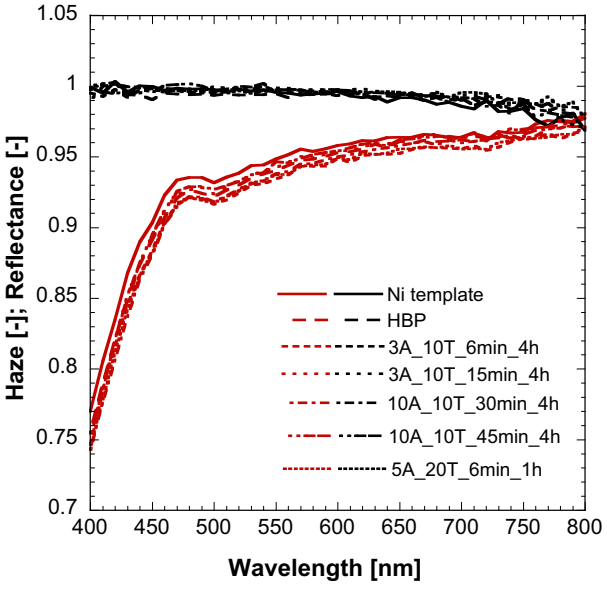

Fig. 6. Haze (black lines) and reflectance (red lines) data for nickel template, HBP and replicated hybrid composite textures. (For interpretation of the references to color in this figure legend, the reader is referred to the web version of this article.)

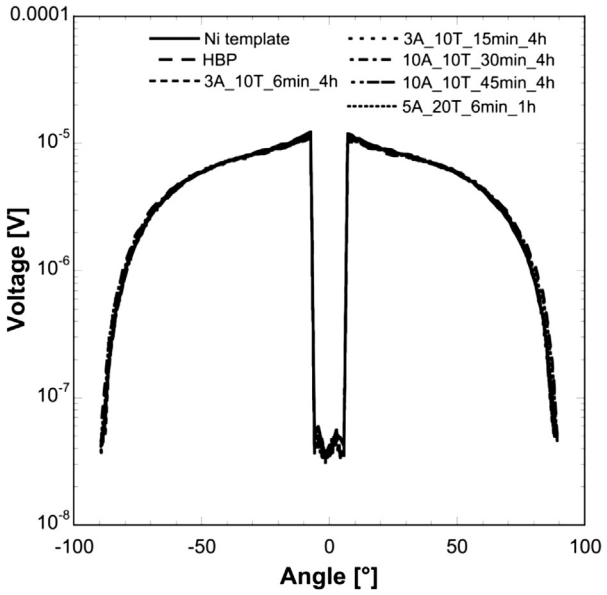

Fig. 7. ARS data for the nickel master, HBP and hybrid composite textures replicas.

of hybrid suspensions was one to two orders of magnitude lower than that of their particulate counterparts. The hybrid nanocomposites were transparent and their hardness reached values up to 287 MPa at a silica fraction of 30 vol%. An optimized dual-cure sequence was devised, where the condensation time before polymerization was decreased for compositions with increasing TEOS. Light-trapping textures were created with perfect shape fidelity up to 25 vol% SiO_2 content using a UVNIL tool with a sub-micron random pyramidal master. The resulting haze was found to be above 99% in the visible light range and the light scattering performance was also very high in a broad angular exposure.

Acknowledgments

The authors would like to acknowledge the PVLab at EPFL for technical assistance for optical characterizations.

References

[1] Drisko GL, Sanchez C. Eur J Inorg Chem 2012;32:5097–105.
[2] Hussain F, Hojjati M, Okamoto M, Gorga RE. J Compos Mater 2006;40(17):1511–75.
[3] Fu S-Y, Feng X-Q, Lauke B, Mai Y-W. Compos Part B: Eng 2008;39:933–61.
[4] Perrin FX, Nguyen V, Vernet JL. Polymer 2002;43(23):6159–67.
[5] Jin J, Lee JJ, Bae BS, Park SJ, Yoo S, Jung K. Org Electron 2012;13(1):53–7.
[6] Mammeri F, Le Bourhis E, Rozes L, Sanchez C. J Mater Chem 2005;15(35–36):3787–811.
[7] Geiser V. Low-stress UV-curable hyperbranched polymer nanocomposites for high-precision devices. PhD thesis #4877. Lausanne: EPFL; 2010.
[8] Schmidt H, Jonschker G, Goedicke S, Mennig M. J Sol-Gel Sci Technol 2000;19(1–3):39–51.
[9] Gonzalez Lazo MA, Teuscher R, Leterrier Y, Månson J-AE, Calderone C, Hessler-Wyser A, et al. Sol Energy Mater Sol Cells 2012;103(0):147–56.
[10] Geiser V, Leterrier Y, Månson J-AE. Macromolecules 2010;43(18):7705–12.
[11] Amerio E, Sangermano M, Malucelli G, Priola A, Voit B. Polymer 2005;46(25):11241–6.
[12] Brinker JC, Scherer GW. Sol-gel science: the physics and chemistry of sol-gel processing. San Diego: Academic Press, Inc.; 1990.
[13] Sarwar M, Zulfiqar S, Ahmad Z. J Sol-Gel Sci Technol 2008;45(1):89–95.
[14] Tsai M-H, Huang S-L, Chiang P-C, Chen C-J. J Appl Polym Sci 2007;106(5):3185–92.
[15] Schottner G. Chem Mater 2001;13(10):3422–35.
[16] Kim JH, Ko JH, Bae BS. J Sol-Gel Sci Technol 2007;41(3):249–55.
[17] Di Gianni A, Trabelsi S, Rizza G, Sangermano M, Althues H, Kaskel S, et al. Macromol Chem Phys 2007;208(1):76–86.
[18] Geiser V, Leterrier Y, Månson J-AE. Macromol Mater Eng 2012;297:155–66.
[19] Lu S-R, Zhang H, Zhao C, Wang X. J Macromol Sci 2005;42:1691–701.
[20] Zou J, Zhao Y, Shi W, Shen X, Nie K. Polym Adv Technol 2005;16(1):55–60.
[21] Ahn SH, Guo LJ. Adv Mater 2008;20(11):2044–9.
[22] Sacks MD, Sheu RS. J Non-Cryst Solids 1987;92(2–3):383–96.
[23] Morpurgo M, Teoli D, Pignatto M, Attrezzi M, Spadaro F, Realdon N. Acta Biomaterialia 2010;6(6):2246–53.
[24] Deckman HW, Wronski CR, Witzke H, Yablonovitch E. Appl Phys Lett 1983;42(11):968–70.
[25] Battaglia C, Soderstrom K, Escarre J, Haug F-J, Domine D, Cuony P, et al. Appl Phys Lett 2010;96(21):213504.
[26] Khan SA, Zoeller NJ. J Rheol 1993;37(6):1225–35.
[27] Ueno K, Inaba A, Kondoh M, Watanabe M. Langmuir 2008;24(10):5253–9.
[28] Zhuravlev LT. Langmuir 1987;3(3):316–8.
[29] Battaglia C, Escarré J, Söderström K, Charrière M, Despeisse M, Haug FJ, et al. Nat Photonics 2011;5(9):535–8.
[30] Söderström K, Escarré J, Cubero O, Haug FJ, Perregaux S, Ballif C. Prog Photovolt Res Appl 2011;19(2):202–10.
[31] Nicole L, Rozes L, Sanchez C. Adv Mater 2010;22(29):3208–14.